Letter

Giant electro-optic and elasto-optic effects in ferroelectric $NbOI_2$

Zhenlong Zhang [1,2] Xuehan Di,[1] Charles Paillard [3,4] Laurent Bellaiche [3,5,*] and Zhijun Jiang [1,2,†]

[1]*Ministry of Education Key Laboratory for Nonequilibrium Synthesis and Modulation of Condensed Matter, Shaanxi Province Key Laboratory of Advanced Functional Materials and Mesoscopic Physics, School of Physics, Xi'an Jiaotong University, Xi'an 710049, China*

[2]*State Key Laboratory of Surface Physics and Department of Physics, Fudan University, Shanghai 200433, China*

[3]*Smart Ferroic Materials Center, Physics Department and Institute for Nanoscience and Engineering, University of Arkansas, Fayetteville, Arkansas 72701, USA*

[4]*Université Paris-Saclay, CentraleSupélec, CNRS, Laboratoire SPMS, 91190 Gif-sur-Yvette, France*

[5]*Department of Materials Science and Engineering, Tel Aviv University, Ramat Aviv, Tel Aviv 6997801, Israel*

(Received 6 June 2024; revised 7 August 2024; accepted 27 August 2024; published 9 September 2024)

First-principles calculations are performed to investigate the electro-optic (EO) and elasto-optic effects of the three-dimensional (bulk) and two-dimensional (monolayer) ferroelectric $NbOI_2$. Remarkably large linear EO and elasto-optic coefficients are discovered in both systems, when under stress-free conditions. We further found that the EO responses of bulk and monolayer $NbOI_2$ can be further enhanced with epitaxial strain, because of a strain-driven ferroelectric-to-paraelectric transition that originates from the softening of some polar optical modes. Our findings thus point out that $NbOI_2$, as well as other niobium oxide dihalides, are highly promising for paving the way for potentially efficient nonlinear optical device applications.

DOI: 10.1103/PhysRevB.110.L100101

The linear electro-optic (EO) effect (or Pockels effect) is defined as the variation of the refractive index of a material affected by an external electrical field [1–3]. It has the potential to be used for power-efficient and high-speed optical devices [4–10], such as EO modulators [11], bistable switches [12], and optical resonators [13]. However, there are very few materials possessing large linear EO effect, which limits its application. The standard material of $LiNbO_3$ is currently the best choice for optical modulators in the telecommunications industry because of its large linear EO coefficient ($\sim$30 pm/V) [3,4]. Finding other materials with even larger EO coefficient is therefore of high importance for practical applications but also for scientific interest by revealing the microscopic reason behind such hypothetical enhancement.

Recently, first-principles calculations predicted very large ferroelectric and piezoelectric effects in the $NbOX_2$ systems [14–16]. These layered niobium oxide dihalides $NbOX_2$ (X = Cl, Br, I) systems were also discovered to exhibit large second-harmonic generation (SHG) likely due to the interplay between anisotropic polarization and excitonic resonance [17–24]. Note that the SHG intensity of $NbOX_2$ family is proportional to the ferroelectric spontaneous polarization, which is highly promising for exploring large second-order optical nonlinearities. However, electro-optic effects, but also elasto-optic conversion that relates a change of strain with a variation in the refractive index, remain relatively unknown in these materials.

The aim of this Letter is to investigate the linear electro-optic effect and elasto-optic effects in stress-free ferroelectric $NbOI_2$ bulk and monolayer, as well as the effect of epitaxial strain on such coupling properties in these systems. As we will see, both $NbOI_2$ bulk and monolayer possess really large EO and elasto-optic coefficients for stress-free conditions, with these responses becoming even giant for some epitaxial strains. The reason behind such enhancement of these nonlinear effects is further revealed.

Here, we choose the ground state structures of ferroelectric $NbOI_2$ bulk and monolayer, which have the $C2$ space group (2 point group) and $Pmm2$ space group ($mm2$ point group), respectively. First-principles calculations are performed on the ferroelectric bulk and monolayer structures based on the density functional theory (DFT) with the generalized gradient approximation of the Perdew-Burke-Ernzerhof (PBE) exchange-correlation functional form, using the ABINIT package [25] with the norm-conserving pseudopotentials [26,27]. We use a Γ-centered $12\times6\times1$ k-point mesh to sample the Brillouin zone of bulk and monolayer $NbOI_2$ and a plane-wave cutoff of 50 hartrees. For the ferroelectric monolayer $NbOI_2$, a vacuum space of more than 20 Å is used to avoid the periodic image interactions. Furthermore, the effects of epitaxial biaxial strain on the structural properties of bulk and monolayer $NbOI_2$ are calculated as well. The considered strains are ranging between -3% and $+3\%$. For each considered strain, the in-plane lattice vectors are kept fixed, while the out-of-plane lattice vector is allowed to relax for bulk $NbOI_2$ but kept fixed for the supercell modeling the monolayer and vacuum. The atomic positions are fully relaxed for both the bulk and monolayer $NbOI_2$ until all the force values acting on the atoms are less than 1×10^{-6} hartree/bohr. In order to mimic the van der Waals (vdW) interactions in $NbOI_2$ bulk, the DFT-D3 method with Becke-Johnson damping [28] was included in the calculations. The strain-induced

*Contact author: laurent@uark.edu
†Contact author: zjjiang@xjtu.edu.cn

structures are then used to calculate the EO tensor, but within the local density approximation (LDA) because such calculation is only implemented within LDA. This method can be rather accurate, since it predicts linear and nonlinear EO coefficients for ferroelectric oxides [29–31] that agree rather well with experimental results [3,32]. Technically, the linear EO tensor r_{ijk} is expressed as

$$\Delta(\varepsilon^{-1})_{ij} = \sum_{k=1}^{3} r_{ijk}\mathcal{E}_k, \tag{1}$$

where $(\varepsilon^{-1})_{ij}$ is the inverse of the electronic dielectric tensor and $\mathcal{E}_k$ is the applied electric field in the Cartesian direction k.

The clamped (strain-free) EO tensor can be written as [29,30]

$$r^{\eta}_{ijk} = r^{\mathrm{el}}_{ijk} + r^{\mathrm{ion}}_{ijk} = \frac{-8\pi}{n_i^2 n_j^2}\chi^{(2)}_{ijk} - \frac{4\pi}{n_i^2 n_j^2\sqrt{\Omega_0}}\sum_m \frac{\alpha^m_{ij} p^m_k}{\omega^2_m}, \tag{2}$$

where r^{el}_{ijk} is the bare electronic contribution, r^{ion}_{ijk} represents the ionic contribution, n_i and n_j are the principal refractive indices, $\chi^{(2)}_{ijk}$ is the nonlinear optical dielectric susceptibility, Ω_0 is the unit cell volume, α^m_{ij} denotes the Raman susceptibility of mode m, p^m_k is the polarity, and ω_m is the phonon mode frequency. Note that the clamped EO tensor and phonon frequencies are directly obtained from density functional perturbation theory (DFPT) calculations [30].

The unclamped (stress-free that adds a piezoelectric contribution) EO coefficients can be expressed as

$$r^{\sigma}_{ijk} = r^{\eta}_{ijk} + \sum_{\alpha,\beta} p_{ij\alpha\beta} d_{k\alpha\beta}, \tag{3}$$

where $p_{ij\alpha\beta}$ is the elasto-optic coefficients and $d_{k\alpha\beta}$ represent the piezoelectric strain coefficients. Note that Eqs. (2) and (3) can be used to calculate the linear clamped and unclamped EO tensor from first principles [33–36]. Measurements with time response method (TRM) [37] and modulation depth method (MDM) [38] can be used to determine the clamped and unclamped EO coefficients.

Moreover, the elasto-optic tensor $p_{ij\alpha\beta}$ is given by the expression [39]

$$\Delta\left(\frac{1}{n^2}\right)_{ij} = \Delta(\varepsilon^{-1})_{ij} = \sum_{\alpha,\beta} p_{ij\alpha\beta} x_{\alpha\beta}, \tag{4}$$

where n is the refractive index (which is simply equal to the square root of the electronic dielectric tensor) and $x_{\alpha\beta}$ denotes the strain tensor.

We first check the structural parameters of $NbOI_2$ bulk and monolayer. The lattice parameters of bulk $NbOI_2$ are found to be $a = 3.89$ Å, $b = 7.51$ Å, $c = 15.15$ Å, and $\alpha = 105.4°$, which are in good agreement with the experimental values of $a = 3.92$ Å, $b = 7.52$ Å, $c = 15.18$ Å, and $\alpha = 105.5°$ [40]. For ferroelectric $NbOI_2$ monolayer, the relaxed lattice constants are $a = 3.94$ Å and $b = 7.58$ Å, which are precisely those found in Refs. [15,20].

Figure 1 displays the crystal structures of the $NbOI_2$ bulk and monolayer, respectively. A spontaneous polarization occurs along the x-axis direction for both ferroelectric $NbOI_2$ bulk and monolayer. The EO tensor of $NbOI_2$ bulk (2 point group) has eight independent elements in the Voigt notation [41]: r_{11}, r_{21}, r_{31}, r_{41}, r_{52}, r_{53}, r_{62}, and r_{63}, while the EO tensor of the $NbOI_2$ monolayer ($mm2$ point group) has five independent elements: r_{11}, r_{21}, r_{31}, r_{53}, and r_{62}. For the $NbOI_2$ monolayer, it is important to recall that the calculated EO tensor predicted by the DFT simulations on the supercell has to be rescaled as [42,43]

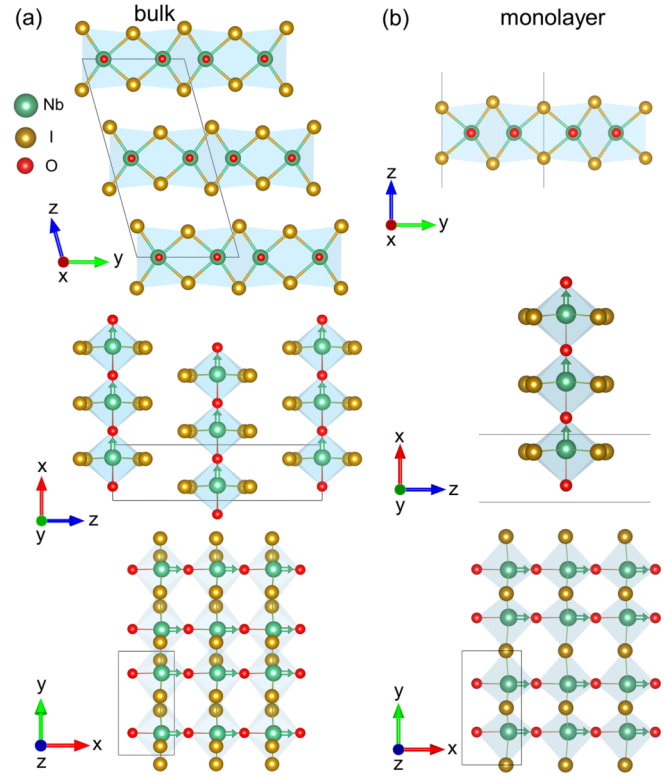

FIG. 1. Crystal structures of ferroelectric $NbOI_2$ bulk and monolayer. Panels (a) and (b) show the side and top views of $NbOI_2$ bulk and monolayer, respectively. Black lines represent the simulated unit cell. The arrows centered on the Nb ions represent the spontaneous polarization direction.

$$r^{\mathrm{2D}}_{11} = \frac{c}{t}\frac{\left(\varepsilon^{\mathrm{SC}}_{11}\right)^2}{\left(\varepsilon^{\mathrm{2D}}_{11}\right)^2} r^{\mathrm{SC}}_{11}, \tag{5}$$

$$r^{\mathrm{2D}}_{21} = \frac{c}{t}\frac{\left(\varepsilon^{\mathrm{SC}}_{22}\right)^2}{\left(\varepsilon^{\mathrm{2D}}_{22}\right)^2} r^{\mathrm{SC}}_{21}, \tag{6}$$

$$r^{\mathrm{2D}}_{31} = \frac{c}{t} r^{\mathrm{SC}}_{31}, \tag{7}$$

$$r^{\mathrm{2D}}_{53} = \frac{\varepsilon^{\mathrm{SC}}_{11}}{\varepsilon^{\mathrm{2D}}_{11}} r^{\mathrm{SC}}_{53}, \tag{8}$$

$$r^{\mathrm{2D}}_{62} = \frac{c}{t}\frac{\varepsilon^{\mathrm{SC}}_{11}\varepsilon^{\mathrm{SC}}_{22}}{\varepsilon^{\mathrm{2D}}_{11}\varepsilon^{\mathrm{2D}}_{22}} r^{\mathrm{SC}}_{62}, \tag{9}$$

where r^{2D}_{11}, r^{2D}_{21}, r^{2D}_{31}, r^{2D}_{53}, and r^{2D}_{62} are the rescaled 2D EO coefficients; r^{SC}_{11}, r^{SC}_{21}, r^{SC}_{31}, r^{SC}_{53}, and r^{SC}_{62} are the EO tensor of the supercell; $\varepsilon^{\mathrm{SC}}_{11}$, $\varepsilon^{\mathrm{SC}}_{22}$, and $\varepsilon^{\mathrm{SC}}_{33}$ are the diagonal elements of the dielectric tensor in the supercell; $\varepsilon^{\mathrm{2D}}_{11}$, $\varepsilon^{\mathrm{2D}}_{22}$, and $\varepsilon^{\mathrm{2D}}_{33}$ are the renormalized 2D dielectric constants; c is the lattice constant of the supercell in monolayer $NbOI_2$, while t is

TABLE I. Clamped electro-optic coefficients in ferroelectric $NbOI_2$ bulk and monolayer.

Bulk EO tensor (pm/V)			Monolayer EO tensor (pm/V)		
58.63	0	0	35.49	0	0
16.17	0	0	8.27	0	0
7.69	0	0	3.98	0	0
0.11	0	0	0	0	0
0	−0.18	0.004	0	0	0.01
0	1.24	−0.09	0	2.36	0

the effective thickness of the 2D material. The choice of t is based on the van der Waals bond length [43,44]. Practically, t is taken to be equal to 7.3 Å here for the $NbOI_2$ monolayer, which is consistent with the experimental report of Ref. [18]. The rescaling of the dielectric constants is given by [44] $\varepsilon_{11}^{2D} = 1 + \frac{c}{t}(\varepsilon_{11}^{SC} - 1)$, $\varepsilon_{22}^{2D} = 1 + \frac{c}{t}(\varepsilon_{22}^{SC} - 1)$, and $\varepsilon_{33}^{2D} = [1 + \frac{c}{t}((\varepsilon_{33}^{SC})^{-1} - 1)]^{-1}$. Note also that the elasto-optic tensor of the monolayer needs to be rescaled in the same way as the EO tensor in 2D systems [43] while the piezoelectric strain coefficients do not need to because they are independent of the thickness of the vacuum layers [16].

Table I shows the clamped electro-optic tensor in ferroelectric $NbOI_2$ bulk and monolayer. Regarding $NbOI_2$ bulk, the predicted clamped EO coefficients are: $r_{11}^{\eta} = 58.63\,\text{pm/V}$, $r_{21}^{\eta} = 16.17\,\text{pm/V}$, $r_{31}^{\eta} = 7.69$ pm/V, $r_{41}^{\eta} = 0.11\,\text{pm/V}$, $r_{52}^{\eta} = -0.18\,\text{pm/V}$, $r_{53}^{\eta} = 0.004\,\text{pm/V}$, $r_{62}^{\eta} = 1.24\,\text{pm/V}$, and $r_{63}^{\eta} = -0.09\,\text{pm/V}$. The largest clamped EO coefficient in $NbOI_2$ bulk is therefore about twice larger than the currently most used EO material $LiNbO_3$ which has a $r_{33}^{\eta} = 30.8\,\text{pm/V}$ [3,29]. For $NbOI_2$ monolayer, the clamped EO coefficients of $r_{11}^{\eta,2D} = 35.49\,\text{pm/V}$, $r_{21}^{\eta,2D} = 8.27\,\text{pm/V}$, and $r_{31}^{\eta,2D} = 3.98\,\text{pm/V}$, are smaller in magnitude than those of bulk. In contrast, the clamped EO coefficients $r_{53}^{\eta,2D}$ and $r_{62}^{\eta,2D}$ of monolayer are larger in magnitude than those of the bulk case but both have small values. Note that the predicted EO coefficients $r_{11}^{\eta,2D}$ in $NbOI_2$ monolayer is also larger than the experimental results in $LiNbO_3$ [3,4] and 2D ferroelectric $CuInP_2S_6$ (with an effective linear EO coefficient to be 20.28 pm/V) [45], which emphasizes the high potential of $NbOI_2$ systems for the design of efficient electro-optic devices.

Table II displays some selected unclamped EO coefficients and elasto-optic coefficients of $NbOI_2$ bulk and monolayer, respectively. For $NbOI_2$ bulk, the largest unclamped EO coefficient of $r_{11}^{\sigma} = 289.76\,\text{pm/V}$, which is about five times larger in magnitude than the clamped one. On the other hand, the values of $r_{21}^{\sigma} = 7.05\,\text{pm/V}$ and $r_{31}^{\sigma} = -12.66\,\text{pm/V}$

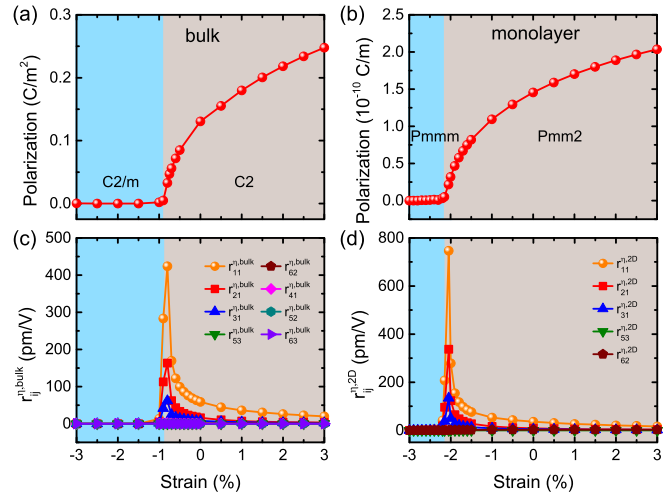

FIG. 2. The polarization P_x as a function of strain in ferroelectric $NbOI_2$ (a) bulk and (b) monolayer, respectively. The clamped EO coefficients as a function of strain in $NbOI_2$ (c) bulk and (d) monolayer, respectively.

are smaller than the clamped one because of the negative piezoelectric contribution. The unclamped EO coefficient of $r_{11}^{\sigma} = 133.63\,\text{pm/V}$ is also large in $NbOI_2$ monolayer, which is about four times stronger than that of the clamped one. The remaining two unclamped EO coefficients in the monolayer case, $r_{21}^{\sigma} = 4.96\,\text{pm/V}$ and $r_{31}^{\sigma} = 3.48\,\text{pm/V}$, are smaller in magnitude than their clamped values due to the negative piezoelectric contribution too.

Let us also indicate that Eq. (4) can be used to obtain accurate elasto-optic coefficients from first-principles calculations. For instance, a first-principles scheme predicted a value of $p_{31} = 0.17$ for bulk $LiNbO_3$ [46], which agrees remarkably well with the experimental value of 0.18 [3]. The presently computed elasto-optic coefficients in $NbOI_2$ bulk are $p_{11} = 1.65$, $p_{21} = 0.61$, and $p_{31} = 0.39$, respectively. The predicted value of p_{11} is therefore very large, namely about four times larger in magnitude than that measured in tetragonal $BaTiO_3$ with $p_{11} = 0.425$ [3]. The magnitude of the predicted p_{31} is more than two times larger in magnitude than that measured in bulk $LiNbO_3$ [3]. The rescaled elasto-optic coefficients in $NbOI_2$ monolayer are also large, with $p_{11} = 1.58$, $p_{21} = 0.46$, and $p_{31} = 0.39$, respectively, which further calls for the use of $NbOI_2$ in technologies taking advantage of elasto-optic conversions.

Let us now investigate the effect of strain on some properties in these promising materials. Figure 2 shows the polarization and clamped EO coefficients as a function of

TABLE II. Unclamped electro-optic and elasto-optic coefficients in ferroelectric $NbOI_2$ bulk and monolayer.

	Unclamped EO tensor (pm/V)			Elasto-optic tensor		
$NbOI_2$	r_{11}^{σ}	r_{21}^{σ}	r_{31}^{σ}	p_{11}	p_{21}	p_{31}
bulk	289.76	7.05	−12.66	1.65	0.61	0.39
monolayer	133.63	4.96	3.48	1.58	0.46	0.39

biaxial epitaxial strain in $NbOI_2$ bulk and monolayer, respectively. As mentioned above, a spontaneous polarization P_x is along the x direction under stress-free conditions in both $NbOI_2$ bulk and monolayer. It is computed from the Berry phase method [47,48]. Note that the calculated spontaneous polarization in $NbOI_2$ monolayer is equal to 145.4 pC/m under stress-free conditions, which is in excellent agreement with previous theoretical values of 142.5 pC/m [15] and 143 pC/m [16]. The behaviors of the polarization and EO coefficients allow the determination of two strain regions for both bulk and monolayer. For strains ranging between $+3\%$ and -0.8% in $NbOI_2$ bulk [Fig. 2(a)], the polarization gradually decreases from 0.25 to 0.03 C/m^2, with the phase retaining its $C2$ space group. In contrast, the phase for strains between -0.9% and -3% has the paraelectric $C2/m$ space group, with therefore no polarization and no finite EO coefficients. For $NbOI_2$ monolayer, the polarization associated with the ferroelectric phase (that has a $Pmm2$ space group) in the range of $+3\%$ to -2.05% decreases from 2.0×10^{-10} to 0.2×10^{-10} C/m [see Fig. 2(b)]. The polarization and EO coefficients are null for strains between -2.1% and -3%, since the resulting phase adopts the paraelectric $Pmmm$ space group.

Let us now pay closer attention to the EO response as a function of strain in $NbOI_2$ bulk and monolayer, as shown in Figs. 2(c) and 2(d). At the boundary between ferroelectric and paraelectric phases in $NbOI_2$ bulk, large values of the clamped EO coefficients $r_{11}^{\eta,\mathrm{bulk}}$ and $r_{21}^{\eta,\mathrm{bulk}}$ are predicted (more than 100 pm/V) due to the strain-driven occurrence of a phase transition from $C2$ to $C2/m$. For the clamped EO coefficients in $NbOI_2$ monolayer, $r_{11}^{\eta,\mathrm{2D}}$ and $r_{21}^{\eta,\mathrm{2D}}$ also show very large values near the boundary between $Pmm2$ and $Pmmm$ phases. Strikingly, such large EO coefficients near this critical strain in both bulk and monolayer are larger than the experimental values in $LiNbO_3$ [3,4] by one order of magnitude—strongly suggesting to employ strained $NbOI_2$ materials for unprecedented electro-optic devices performance.

Four lowest phonon modes, expressed as $B_u^{(4)}$, $B^{(4)}$, $B_{3u}^{(4)}$, and $B_1^{(4)}$ [see Figs. 3(a) and 3(b)] are important in $NbOI_2$ bulk and monolayer. As a matter of fact, for $NbOI_2$ bulk, Fig. 3(a) reveals that the $B^{(4)}$ phonon mode becomes very soft around the strain $\sim -0.8\%$, which corresponds to the boundary between $C2$ (ferroelectric) and $C2/m$ (paraelectric) phases. Having some frequencies approaching zero is a guarantee to have large EO response, as indicated by the second term of Eq. (2). Indeed, we numerically found that the main contribution of phonon modes for the largest $r_{11}^{\eta,\mathrm{bulk}}$ EO coefficient mostly arises from the polar mode $B^{(4)}$. Figure 3(c) displays the atomic displacement of such mode at -0.8% strain, with the Nb ions displacing along the [100] direction while O and I ions move along the opposite $[\bar{1}00]$ direction in $NbOI_2$ bulk.

For $NbOI_2$ monolayer, the continuous evolution from the ferroelectric $Pmm2$ phase to the paraelectric $Pmmm$ state is driven by a softening of the $B_1^{(4)}$ and $B_{3u}^{(4)}$ modes. At the phase boundary of -2.05% strain, the largest $r_{11}^{\eta,\mathrm{2D}}$ coefficient now mostly stems from the polar mode we denote as $B_1^{(4)}$, which shows a similar atomic character of eigenvector [see Fig. 3(d)] as the mode $B^{(4)}$ of bulk case. One can thus safely conclude that, in both strained $NbOI_2$ bulk and monolayer, the large linear EO coefficients mainly originate from a strain-induced softening of the lowest polar mode and a resulting ferroelectric-to-paraelectric phase transition.

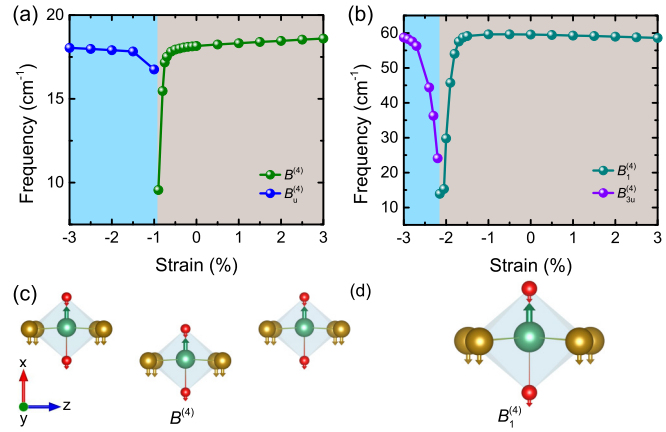

FIG. 3. The frequency of selected phonon modes as a function of strain in ferroelectric (a) bulk and (b) monolayer $NbOI_2$, respectively. Panels (c) and (d) show the atomic character of the eigenvector of modes $B^{(4)}$ and $B_1^{(4)}$ in $NbOI_2$ bulk and monolayer, respectively.

In summary, we investigated linear electro-optic and elasto-optic effects in $NbOI_2$ bulk and monolayer from first-principles calculations. We predict large clamped and unclamped EO and elasto-optic coefficients in both stress-free bulk and monolayer. We also revealed the effect of epitaxial strain on the EO response of $NbOI_2$ bulk and monolayer. In particular, in both systems, a strain-induced ferroelectric-to-paraelectric phase transition is discovered, being driven by a softening of some lowest phonon modes and which results in very large linear EO responses. The phase transitions and large EO responses are accompanied by changes in the atomic bond length and electronic band gap (see the Supplemental Material (SM) [49]). The SM [49] further demonstrates that other $NbOX_2$ materials, namely $NbOBr_2$ and $NbOCl_2$, can also hold these spectacular effects. We compare the electro-optic and elasto-optic coefficients in $NbOI_2$ bulk and monolayer with other ferroelectric materials [49] and find that $NbOI_2$ has the best performance. Note that the phonon dispersions and stability are also discussed in the SM [49]. We thus hope that the present study will encourage the experimental investigation of electro-optic and elasto-optic effects in bulk and 2D ferroelectric niobium oxide dihalides.

This work is supported by the National Natural Science Foundation of China (Grant No. 12374092), the Natural Science Basic Research Program of Shaanxi (Program No. 2023-JC-YB-017), the Shaanxi Fundamental Science Research Project for Mathematics and Physics (Grant No. 22JSQ013), the "Young Talent Support Plan" of Xi'an Jiaotong University (Grant No. WL6J004), the Open Project of State Key Laboratory of Surface Physics (Grant No. KF2023_06), the Fundamental Research Funds for the Central Universities, and the HPC Platform of Xi'an Jiaotong University. C.P. acknowledges partial support through Agence Nationale de la Recherche through Grant Agreement No. ANR-23-CE09-0007 (SOFIANE) and the Air Force Office of

Scientific Research through Award No. FA9550-24-1-0263. C.P. and L.B. thank the Defense Advanced Research Projects Agency Defense Sciences Office (DARPA-DSO) Program: Accelerating discovery of Tunable Optical Materials (ATOM) under Agreement No. HR00112390142 and the Office of the Secretary of Defense for Research and Engineering under Award No. FA9550-23-1-0500. L.B. also acknowledges the MonArk NSF Quantum Foundry supported by the National Science Foundation Q-AMASE-i Program under NSF Award No. DMR-1906383, the ARO Grant No. W911NF-21–1–0113, and the Vannevar Bush Faculty Fellowship (VBFF) Grant No. N00014-20-1–2834 from the Department of Defense.

Z.Z. and X.D. contributed equally to this work.

[1] M. DiDomenico, Jr. and S. H. Wemple, Oxygen-octahedra ferroelectrics. I. theory of electro-optical and nonlinear optical effects, J. Appl. Phys. **40**, 720 (1969).

[2] S. H. Wemple and M. DiDomenico, Jr., Oxygen-octahedra ferroelectrics. II. Electro-optical and nonlinear-optical device applications, J. Appl. Phys. **40**, 735 (1969).

[3] M. J. Weber, *Handbook of Optical Materials* (CRC Press, Boca Raton, FL, 2002).

[4] E. H. Turner, High-frequency electro-optic coefficients of lithium niobate, Appl. Phys. Lett. **8**, 303 (1966).

[5] M. E. Lines and A. M. Glass, *Principles and Applications of Ferroelectrics and Related Materials* (Oxford University Press, New York, 1977).

[6] S. H. Wemple and M. DiDomenico, Jr., Electrooptical and nonlinear optical properties of crystals, Appl. Solid State Sci. **3**, 263 (1972).

[7] B. E. A. Saleh and M. C. Teich, *Fundamentals of Photonics* (Wiley, New York, 1991).

[8] A. Yariv and P. Yeh, *Photonics: Optical Electronics in Modern Communications* (Oxford University Press, New York, 2007).

[9] R. W. Boyd, *Nonlinear Optics*, 3rd ed. (Academic Press, New York, 2008).

[10] M. Bass, *Handbook of Optics: Volume IV-Optical Properties of Materials, Nonlinear Optics, Quantum Optics*, 3rd ed. (McGraw-Hill Education, New York, 2010).

[11] Q. Xu, B. Schmidt, S. Pradhan, and M. Lipson, Micrometre-scale silicon electro-optic modulator, Nature (London) **435**, 325 (2005).

[12] R. Martínez-Lorente, J. Parravicini, M. Brambilla, L. Columbo, F. Prati, C. Rizza, A. J. Agranat, and E. DelRe, Scalable electro-optic control of localized bistable switching in broad-area VCSELs using reconfigurable funnel waveguides, Phys. Rev. Appl. **7**, 064004 (2017).

[13] A. Guarino, G. Poberaj, D. Rezzonico, R. Degl'Innocenti, and P. Günter, Electro–optically tunable microring resonators in lithium niobate, Nat. Photon. **1**, 407 (2007).

[14] Y. Jia, M. Zhao, G. Gou, X. C. Zeng, and J. Li, Niobium oxide dihalides $NbOX_2$: A new family of two-dimensional van der Waals layered materials with intrinsic ferroelectricity and antiferroelectricity, Nanoscale Horiz. **4**, 1113 (2019).

[15] Q. Ye, Y.-H. Shen, and C.-G. Duan, Ferroelectric controlled spin texture in two-dimensional $NbOI_2$ monolayer, Chin. Phys. Lett. **38**, 087702 (2021).

[16] Y. Wu, I. Abdelwahab, K. C. Kwon, I. Verzhbitskiy, L. Wang, W. H. Liew, K. Yao, G. Eda, K. P. Loh, L. Shen, and S. Y. Quek, Data-driven discovery of high performance layered van der Waals piezoelectric $NbOI_2$, Nat. Commun. **13**, 1884 (2022).

[17] Y. Fang, F. Wang, R. Wang, T. Zhai, and F. Huang, 2D $NbOI_2$: A chiral semiconductor with highly in-plane anisotropic electrical and optical properties, Adv. Mater. **33**, 2101505 (2021).

[18] I. Abdelwahab, B. Tilmann, Y. Wu, D. Giovanni, I. Verzhbitskiy, M. Zhu, R. Berté, F. Xuan, L. d. S. Menezes, G. Eda, T. C. Sum, S. Y. Quek, S. A. Maier, and K. P. Loh, Giant second-harmonic generation in ferroelectric $NbOI_2$, Nat. Photon. **16**, 644 (2022).

[19] J. Fu, N. Yang, Y. Liu, Q. Liu, J. Du, Y. Fang, J. Wang, B. Gao, C. Xu, D. Zhang, A. J. Meixner, G. Gou, F. Huang, L. Zhen, and Y. Li, Emission dipole and pressure-driven tunability of second harmonic generation in vdWs ferroelectric $NbOI_2$, Adv. Funct. Mater. **34**, 2308207 (2024).

[20] L. Ye, W. Zhou, D. Huang, X. Jiang, Q. Guo, X. Cao, S. Yan, X. Wang, D. Jia, D. Jiang, Y. Wang, X. Wu, X. Zhang, Y. Li, H. Lei, H. Gou, and B. Huang, Manipulation of nonlinear optical responses in layered ferroelectric niobium oxide dihalides, Nat. Commun. **14**, 5911 (2023).

[21] Q. Guo, X.-Z. Qi, L. Zhang, M. Gao, S. Hu, W. Zhou, W. Zang, X. Zhao, J. Wang, B. Yan, M. Xu, Y.-K. Wu, G. Eda, Z. Xiao, S. A. Yang, H. Gou, Y. P. Feng, G.-C. Guo, W. Zhou, X.-F. Ren *et al.*, Ultrathin quantum light source with van der Waals $NbOCl_2$ crystal, Nature (London) **613**, 53 (2023).

[22] H. Wang, Q. Chen, Y. Cao, W. Sang, F. Tan, H. Li, T. Wang, Y. Gan, D. Xiang, and T. Liu, Anisotropic strain-tailoring nonlinear optical response in van der Waals $NbOI_2$, Nano Lett. **24**, 3413 (2024).

[23] Q. Yan, Y. Weng, S. Wang, Z. Zhou, Y. Hu, Q. Li, J. Xue, Z. Feng, Z. Luo, R. Feng, L. You, and L. Fang, Ambient degradation anisotropy and mechanism of van der Waals ferroelectric $NbOI_2$, ACS Appl. Mater. Interfaces **16**, 9051 (2024).

[24] W. Chen, S. Zhu, R. Duan, C. Wang, F. Wang, Y. Wu, M. Dai, J. Cui, S. H. Chae, Z. Li, X. Ma, Q. Wang, Z. Liu, and Q. J. Wang, Extraordinary enhancement of nonlinear optical interaction in $NbOBr_2$ microcavities, Adv. Mater. **36**, 2400858 (2024).

[25] X. Gonze, J.-M. Beuken, R. Caracas, F. Detraux, M. Fuchs, G.-M. Rignanese, L. Sindic, M. Verstraete, G. Zerah, F. Jollet, M. Torrent, A. Roy, M. Mikami, Ph. Ghosez, J.-Y. Raty, and D. C. Allan, First-principles computation of material properties: The ABINIT software project, Comput. Mater. Sci. **25**, 478 (2002).

[26] D. R. Hamann, Optimized norm-conserving Vanderbilt pseudopotentials, Phys. Rev. B **88**, 085117 (2013).

[27] M. J. van Setten, M. Giantomassi, E. Bousquet, M. J. Verstraete, D. R. Hamann, X. Gonze, and G.-M. Rignanese, The PseudoDojo: Training and grading a 85 element optimized norm-conserving pseudopotential table, Comput. Phys. Commun. **226**, 39 (2018).

[28] S. Grimme, S. Ehrlich, and L. Goerigk, Effect of the damping function in dispersion corrected density functional theory, J. Comput. Chem. **32**, 1456 (2011).

[29] M. Veithen, X. Gonze, and Ph. Ghosez, First-principles study of the electro-optic effect in ferroelectric oxides, Phys. Rev. Lett. **93**, 187401 (2004).

[30] M. Veithen, X. Gonze, and Ph. Ghosez, Nonlinear optical susceptibilities, Raman efficiencies, and electro-optic tensors from first-principles density functional perturbation theory, Phys. Rev. B **71**, 125107 (2005).

[31] Z. Jiang, C. Paillard, H. Xiang, and L. Bellaiche, Linear versus nonlinear electro-optic effects in materials, Phys. Rev. Lett. **125**, 017401 (2020).

[32] L. Chen, Y. Zhang, Q. Guo, D. Zhang, X. Zhong, and J. Yuan, Terahertz electro-optic properties of $PbZr_{0.52}Ti_{0.48}O_3$ and $BaTiO_3$ ferroelectric thin films, Appl. Phys. Lett. **105**, 112903 (2014).

[33] C. Paillard, S. Prokhorenko, and L. Bellaiche, Strain engineering of electro-optic constants in ferroelectric materials, npj Comput. Mater. **5**, 6 (2019).

[34] Z. Jiang, C. Paillard, D. Vanderbilt, H. Xiang, and L. Bellaiche, Designing multifunctionality via assembling dissimilar materials: Epitaxial AlN/ScN superlattices, Phys. Rev. Lett. **123**, 096801 (2019).

[35] T. Paoletta and A. A. Demkov, Pockels effect in low-temperature rhombohedral $BaTiO_3$, Phys. Rev. B **103**, 014303 (2021).

[36] S. Prosandeev, C. Paillard, and L. Bellaiche, Crossover from linear to quadratic electro-optic behavior in $BaTiO_3$ and (Ba, Sr)TiO_3 solid solution, Phys. Rev. Lett. **132**, 196901 (2024).

[37] M. Abarkan, M. Aillerie, N. Kokanyan, C. Teyssandier, and E. Kokanyan, Electro-optic and dielectric properties of zirconium-doped congruent lithium–niobate crystals, Opt. Mater. Express **4**, 179 (2014).

[38] M. Abarkan, A. Danielyan, N. Kokanyan, M. Aillerie, S. Kostritskii, and E. Kokanyan, The clamped and unclamped effective electro-optic coefficients of zirconium-doped congruent lithium niobate crystals, J. Phys.: Conf. Ser. **879**, 012004 (2017).

[39] M. Zgonik, P. Bernasconi, M. Duelli, R. Schlesser, P. Günter, M. H. Garrett, D. Rytz, Y. Zhu, and X. Wu, Dielectric, elastic, piezoelectric, electro-optic, and elasto-optic tensors of $BaTiO_3$ crystals, Phys. Rev. B **50**, 5941 (1994).

[40] J. Rijnsdorp and F. Jellinek, The crystal structure of niobium oxide diiodide $NbOI_2$, J. Less-Common Met. **61**, 79 (1978).

[41] J. F. Nye, *Physical Properties of Crystals: Their Representation by Tensors and Matrices* (Oxford University Press, Oxford, 1985).

[42] Z. Jiang, C. Paillard, H. O. H. Churchill, M. Xia, S. Zhang, H. Xiang, and L. Bellaiche, Large linear and nonlinear electro-optic coefficients in two-dimensional ferroelectrics, Phys. Rev. B **106**, L081404 (2022).

[43] Z. Jiang, H. Xiang, L. Bellaiche, and C. Paillard, Electro-optic properties from *ab initio* calculations in two-dimensional materials, Phys. Rev. B **109**, 165414 (2024).

[44] A. Laturia, M. L. Van de Put, and W. G. Vandenberghe, Dielectric properties of hexagonal boron nitride and transition metal dichalcogenides: From monolayer to bulk, npj 2D Mater. Appl. **2**, 6 (2018).

[45] Y. Liu, Y. Wu, R. Duan, J. Fu, M. Ovesen, S. C. E. Lai, T.-E. Yeo, J. Y. Chee, Y. Chen, S. L. Teo, H. R. Tan, W. Zhang, J. K. W. Yang, K. S. Thygesen, Z. Liu, Y.-W. Zhang, and J. Teng, Linear electro-optic effect in 2D ferroelectric for electrically tunable metalens, Adv. Mater. **36**, 2401838 (2024).

[46] L. Chen, Y. Yang, Z. Gui, D. Sando, M. Bibes, X. K. Meng, and L. Bellaiche, Large elasto-optic effect in epitaxial $PbTiO_3$ films, Phys. Rev. Lett. **115**, 267602 (2015).

[47] R. D. King-Smith and D. Vanderbilt, Theory of polarization of crystalline solids, Phys. Rev. B **47**, 1651(R) (1993).

[48] R. Resta, Macroscopic polarization in crystalline dielectrics: the geometric phase approach, Rev. Mod. Phys. **66**, 899 (1994).

[49] See Supplemental Material at http://link.aps.org/supplemental/10.1103/PhysRevB.110.L100101 for more details about (i) the bond length and electronic band gap in $NbOI_2$ bulk and monolayer; (ii) phonon dispersions and stability in $NbOI_2$ bulk and monolayer; (iii) electro-optic and elasto-optic effects in $NbOBr_2$ and $NbOCl_2$ bulks and monolayers under stress-free conditions; and (iv) strain-induced polarization and electro-optic responses in $NbOBr_2$ and $NbOCl_2$ bulks and monolayers, which includes Refs. [3,4,14,20,21,24,30,45,46,50].

[50] J. Beck and C. Kusterer, Crystal structure of $NbOBr_2$, Z. Anorg. Allg. Chem. **632**, 2193 (2006).